Acta Oceanologica Sinica, Vol. 15, No. 3, pp. 283 ~296, 1996. ISSN 0253-505X

Published by China Ocean Press.

A BFG model for calculation of tidal current and diffusion of pollutants in nearshore areas*

Shi Fengyan[1] and Zheng Lianyuan[2]

(*Received December* 3, 1995; *accepted January* 1, 1996)

Abstract——This study presents a boundary-fitted grid (BFG) numerical model with an aim to simulate the tidal currents and diffusion of pollutants in complicated nearshore areas. To suit the general model to any curvilinear grids, generalized 2-D shallow sea dynamic equations and the advection diffusion equation are derived in curvilinear coordinates, and the contravariant components of the velocity vector are adopted for easily realizing boundary conditions and making the equations conservational. As the generalized equations are not limited by a specific coordinate transformation, a self-adaptive grid generation method is then proposed conveniently to generate a boundary-fitted and varying spacing grid. The calculation in the Yangpu Bay and the Xinying Bay shows that this is an effective model for calculating tidal currents and diffusion of pollutants in the more complicated nearshore areas.

Key words BFG model, numerical calculation, shallow sea equations and advection diffusion equation in curvilinear coordinates

---

* This project was supported by the Excellent Talent Foundation across the Century of State Educational Commission.

1. State Key Laboratory of Estuarine and Coastal Research, Institute of Estuarine and Coastal Research, East China Normal University, Shanghai 200062, China

2. Department of Marine Sciences, the University of Georgia, Athens, GA 30602-2206, U.S.A.

INTRODUCTION

The numerical models with uniform rectangular grids are generally used to calculate tidal motions and diffusion of pollutants, and these models show a fairly accuracy in the calculations in shallow areas with smooth coastlines and topographies. This kind of models, however, are unsatisfactory when they are used in more complex nearshore areas because it is difficult to design the uniform grids to fit the complex boundaries and topographies. A typical case of such areas is a small bay connected by a narrow channel, and the width of the channel is even smaller than the generally used grid spacing. Though fine grid can be used in this case, the computation quantity may greatly increase because of the increase in the grid number and the decrease in the time step. So it is of importance to generate a curvilinear grid mesh which is fine in nearshore areas and coarse in offshore areas. In recent years, the finite element method (FEM) (Lynch and Gray, 1980), boundary element method (BEM) (Medina *et al.*, 1991) and boundary fitted grid (BFG) method (Dortch *et al.*, 1992) are used in the numerical calculation involving shallow sea dynamics. And among these, the BFG method is more widely used for its superiority of using the mature finite difference scheme. Two examples of this kind of BFG models are self-adaptive grid model (SAM) and wet-dry grid point model in curvilinear grids (WDM), which are proposed by Shi and Sun (1995, 1996) recently in the calculation of storm surge flooding. In the SAM model, a generalized coordinate transformation with a time term is adopted to generate a moving coordinate fitted to moving boundaries all the time. And the WDM model employs a coordinate transformation, which is independent of time, to generate a fixed grid mesh fitting to dykes and topographies, and wet-dry grid point criterion is thus employed for controlling the motions of boundaries. The WDM model is considered a simple and economic model for dealing with more complex nearshore areas.

In the present paper, the same coordinate transformation as that in the WDM model is adopted to derive a set of governing equations of tidal motions and the advection diffusion equation of pollutants in generalized curvilinear coordinates. In the equations, the contravariant components of the velocity vector are employed for easily realizing boundary conditions and making the transformed equations conservational, which is convenient for finite differential discretizations.

The self-adaptive grid generation method (Brackbill and Saltzman, 1982) is also employed in the present paper to generate a boundary-fitted and varying spacing grid mesh which is suitable for more complicated nearshore areas. The present BFG model is finally used in the calculation in the Yangpu Bay and the Xinying Bay, between which there is a narrow channel, and the verification calculation shows that the densified grid in the complex area, especially in the narrow channel, makes the calculation more accurate.

EQUATIONS ON THE CURVILINEAR COORDINATES

In rectangular Cartesian coordinates, the 2-D governing equations of tidal motions can be described as

$$\frac{\partial H}{\partial t} + \frac{\partial Hu}{\partial x} + \frac{\partial Hv}{\partial y} = 0, \tag{1}$$

$$\frac{\partial u}{\partial t} + u\frac{\partial u}{\partial x} + v\frac{\partial u}{\partial y} - fv = -g\frac{\partial \zeta}{\partial x} - \frac{ku}{H}(u^2 + v^2)^{1/2}, \tag{2}$$

$$\frac{\partial v}{\partial t} + u\frac{\partial v}{\partial x} + v\frac{\partial v}{\partial y} + fu = -g\frac{\partial \zeta}{\partial y} - \frac{kv}{H}(u^2 + v^2)^{1/2}, \tag{3}$$

where u and v are the depth-averaged components of velocity; f denotes the Coriolis parameter; the pressure is taken as hydrostatic and the effects of astronomical tide-generating forces and barometric forcings are omitted; ζ denotes the surface elevation; $H = h + \zeta$, h is the depth from the undisturbed sea level to the sea-floor; the bottom stress is parameterized in terms of a quadratic law; and ρ denotes the water density.

The advection diffusion equation of the depth-averaged concentration of pollutants P can be described as

$$\frac{\partial HP}{\partial t} + \frac{\partial HuP}{\partial x} + \frac{\partial HvP}{\partial y} - \frac{\partial}{\partial x}(HK_x\frac{\partial P}{\partial x}) - \frac{\partial}{\partial y}(HK_y\frac{\partial P}{\partial y}) = HS, \tag{4}$$

where K_x and K_y denote horizontal diffusivity, and $(K_x, K_y) = 5.93\,Hg^{1/2}/C(u, v)$, C is the Chezy coeffecient; S is the production term which is the mass of pollutants released in a unit volume per second.

Lateral boundary conditions, i.e., the normal velocity on the boundary is zero and the normal diffusion of pollutants is zero if there is no pollutant source on the boundary, can be described as follows:

$$v_n = 0, \tag{5}$$

$$\frac{\partial P}{\partial n} = 0. \tag{6}$$

On open boundaries, tidal elevations are generally given as the open boundary condition of tidal motions. And the concentration P is written as follows:

$$P = 0 \qquad \text{(inflow)}, \tag{7}$$

$$\frac{\partial P}{\partial t} + v_n \frac{\partial P}{\partial n} = 0 \qquad \text{(outflow)}. \tag{8}$$

A general coordinate transformation is introduced then:

$$\xi = \xi(x, y), \qquad \eta = \eta(x, y). \tag{9}$$

It should be noted that the transformation is independent of time, which is different from the transformation chosen in the SAM method. So the transformed coordinate is fixed in the calculated region. The chosen boundaries Γ_1, Γ_2, Γ_3 and Γ_4 in the physical plane thus become Π_1, Π_2, Π_3 and Π_4 respectively in the image plane as shown in Fig. 1.

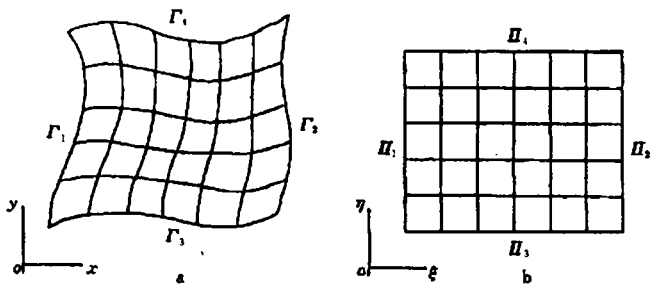

Fig. 1. Physical plane (a) and transformed image plane (b).

To realize the boundary conditions conveniently in the image plane, the general components of the velocity, i.e., contravariant components of the velocity vector, are introduced as follows:

$$U = \frac{\mathrm{d}\xi}{\mathrm{d}t} = u \frac{\partial \xi}{\partial x} + v \frac{\partial \xi}{\partial y}, \tag{10}$$

$$V = \frac{\mathrm{d}\eta}{\mathrm{d}t} = u \frac{\partial \eta}{\partial x} + v \frac{\partial \eta}{\partial y}, \tag{11}$$

and by using the following relations:

$$\xi_x = \frac{y_\eta}{J}, \qquad \xi_y = \frac{-x_\eta}{J}, \qquad \eta_x = \frac{-y_\xi}{J}, \qquad \eta_y = \frac{x_\xi}{J},$$

where J is the Jacobian value of the coordinate transformation, i.e., $J = x_\xi y_\eta - x_\eta y_\xi$, Eqs (10)

and (11) then become the new representations in the image plane:

$$U = \frac{1}{J}(uy_\eta - vx_\eta), \tag{12}$$

$$V = \frac{1}{J}(-uy_\xi + vx_\xi). \tag{13}$$

Equations (12) and (13) may show apparently physical meaning of the components U and V if they are taken as representations of vector forms. So, a set of unit vectors is defined as

$$X_1 = \frac{y_\eta \boldsymbol{i} - x_\eta \boldsymbol{j}}{\sqrt{\alpha}}, \qquad X_2 = \frac{-y_\xi \boldsymbol{i} + x_\xi \boldsymbol{j}}{\sqrt{\gamma}},$$

where $\alpha = x_\eta^2 + y_\eta^2$, $\gamma = x_\xi^2 + y_\xi^2$. It is clear that X_1 and X_2 are the unit normal vectors on the coordinate curve line $\xi = \text{const}$ and $\eta = \text{const}$ respectively. Equations (12) and (13) may be represented then as follows:

$$\boldsymbol{V} \cdot X_1 = \frac{UJ}{\sqrt{\alpha}}, \tag{14}$$

$$\boldsymbol{V} \cdot X_2 = \frac{VJ}{\sqrt{\gamma}}, \tag{15}$$

where $\boldsymbol{V} = u\boldsymbol{i} + v\boldsymbol{j}$. Equations (14) and (15) show that $UJ/\sqrt{\alpha}$ is the normal projection of $\boldsymbol{V}$ on the curve line $\xi = \text{const}$ and $VJ/\sqrt{\gamma}$ the normal projection of $\boldsymbol{V}$ on the curve line $\eta = \text{const}$. So U and V can defined as the general velocities along normal directions of the curvilinear coordinates.

To a physical variable F, its partial difference with respect to the coordinates in the physical plane (x, y) can be transformed into the following representations in the image plane (ξ, η):

$$\frac{\partial F}{\partial x} = \frac{\partial F}{\partial \xi}\xi_x + \frac{\partial F}{\partial \eta}\eta_x = \frac{1}{J}\left(\frac{\partial F}{\partial \xi}y_\eta - \frac{\partial F}{\partial \eta}y_\xi\right), \tag{16}$$

$$\frac{\partial F}{\partial y} = \frac{\partial F}{\partial \xi}\xi_y + \frac{\partial F}{\partial \eta}\eta_y = \frac{1}{J}\left(-\frac{\partial F}{\partial \xi}x_\eta + \frac{\partial F}{\partial \eta}x_\xi\right). \tag{17}$$

By using Eqs (12), (13), (16) and (17), Eqs (1), (2) and (3) may be transformed into the following forms in the image plane:

$$J\frac{\partial \zeta}{\partial t} + \frac{\partial HUJ}{\partial \xi} + \frac{\partial HVJ}{\partial \eta} = 0, \tag{18}$$

$$\frac{\partial \tilde{u}}{\partial t} + \frac{\partial \tilde{u}U}{\partial \xi} + \frac{\partial \tilde{u}V}{\partial \eta} - f\tilde{v} = -gH\left(y_\eta \frac{\partial \zeta}{\partial \xi} - y_\xi \frac{\partial \zeta}{\partial \eta}\right) - k\frac{\sqrt{u^2 + v^2}}{H}\tilde{u}, \tag{19}$$

$$\frac{\partial \tilde{v}}{\partial t} + \frac{\partial \tilde{v}U}{\partial \xi} + \frac{\partial \tilde{v}V}{\partial \eta} + f\tilde{u} = -gH\left(-x_\eta \frac{\partial \zeta}{\partial \xi} + x_\xi \frac{\partial \zeta}{\partial \eta}\right) - k\frac{\sqrt{u^2 + v^2}}{H}\tilde{v}, \tag{20}$$

where

$$\tilde{u} = HJu, \qquad \tilde{v} = HJv. \tag{21}$$

Equation (4) may be transformed into the final equation in the image plane by means of Eqs (12), (13), (16), (17) and (18):

$$\frac{\partial JHP}{\partial t} + \frac{\partial JHUP}{\partial \xi} + \frac{\partial JHVP}{\partial \eta} = \frac{\partial C_1}{\partial \xi} y_\eta + \frac{\partial C_2}{\partial \xi} x_\eta - \frac{\partial C_1}{\partial \eta} y_\xi - \frac{\partial C_2}{\partial \eta} x_\xi + HJS, \tag{22}$$

where

$$C_1 = \frac{K_x H}{J}(P_\xi y_\eta - P_\eta y_\xi), \qquad C_2 = \frac{K_y H}{J}(P_\xi x_\eta - P_\eta x_\xi). \tag{23}$$

The lateral boundary condition of tidal motions thus can be described as a simple representation in the image plane by means of Eqs (14) and (15):

$$U = 0 \qquad \text{at } \Pi_1 \text{ and } \Pi_2, \tag{24}$$

$$V = 0 \qquad \text{at } \Pi_3 \text{ and } \Pi_4. \tag{25}$$

The lateral boundary condition of the concentration P thus becomes

$$P_\xi - \frac{\beta}{\alpha} P_\eta = 0 \qquad \text{at } \Pi_1 \text{ and } \Pi_2, \tag{26}$$

$$P_\eta - \frac{\beta}{\gamma} P_\xi = 0 \qquad \text{at } \Pi_3 \text{ and } \Pi_4, \tag{27}$$

where $\beta = x_\xi x_\eta + y_\xi y_\eta$. For the rectangular grids on the boundary, $\beta = 0$, Eqs (26) and (27) thus can be described in the simple forms:

$$P_\xi = 0 \qquad \text{at } \Pi_1 \text{ and } \Pi_2, \tag{28}$$

$$P_\eta = 0 \qquad \text{at } \Pi_3 \text{ and } \Pi_4. \tag{29}$$

The open boundary condition of concentration P can be represented as

$$P = 0 \qquad \text{(inflow)}, \tag{30}$$

and

$$\frac{\partial P}{\partial t} + U\frac{\partial P}{\partial \xi} - U\frac{\beta}{\alpha}\frac{\partial P}{\partial \eta} = 0 \qquad \text{(outflow, at } \Pi_1 \text{ and } \Pi_2), \tag{31}$$

$$\frac{\partial P}{\partial t} + V\frac{\partial P}{\partial \eta} - V\frac{\beta}{\gamma}\frac{\partial P}{\partial \xi} = 0 \qquad \text{(outflow, at } \Pi_3 \text{ and } \Pi_4). \tag{32}$$

To the rectangular grids on the boundary, Eqs (31) and (32) become

$$\frac{\partial P}{\partial t} + U\frac{\partial P}{\partial \xi} = 0 \qquad \text{(outflow, at } \Pi_1 \text{ and } \Pi_2), \tag{33}$$

$$\frac{\partial P}{\partial t} + V\frac{\partial P}{\partial \eta} = 0 \qquad \text{(outflow, at } \Pi_3 \text{ and } \Pi_4\text{)}. \tag{34}$$

Equations (18), (19), (20) and (22) are generalized equations applicable to any kind of curvilinear coordinates because they are independent of any specific transformation. The computational grid may be generated by any method such as the algebraic transformation, the differential transformation and even the artificial ones.

NUMERICAL GRID GENERATION

In terms of the calculations in more complex nearshore areas, it is necessary to generate boundary-fitted and varying spacing grids for improving calculating accuracy and numerical stability. Smoothness and orthogonality of grids are also important for the computational accuracy. In addition, the orthogonal grid on boundaries is convenient for realizing the orthogonal boundary conditions as described in Eqs (28), (29), (33) and (34). Even if the grid on boundaries is not exactly orthogonal, the more orthogonal grid will benefit explicit discretizations of Eqs (26), (27), (31) and (32).

Brackbill and Saltzman (1982) proposed a unmerical generation method optimizing simultaneously grids variation in cell volumes, grid smoothness and orthogonality. The main idea is that minimizing the functions by which the three properties are measured results in a set of Euler equations which are satisfied by the coordinate values of grid points as the image of a mapping $x(\xi, \eta)$ or $y(\xi, \eta)$. The Euler equations are

$$b_1 x_{\xi\xi} + b_2 x_{\xi\eta} + b_3 x_{\eta\eta} + a_1 y_{\xi\xi} + a_2 y_{\xi\eta} + a_3 y_{\eta\eta} = -\lambda_v J^2 \frac{\partial W}{\partial x}, \tag{35}$$

$$a_1 x_{\xi\xi} + a_2 x_{\xi\eta} + a_3 x_{\eta\eta} + c_1 y_{\xi\xi} + c_2 y_{\xi\eta} + c_3 y_{\eta\eta} = -\lambda_v J^2 \frac{\partial W}{\partial y}, \tag{36}$$

where a_i, b_i and $c_i (i = 1, 2, 3)$ are the differentiation of (x, y) with respect to (ξ, η) [see Brackbill and Saltzman (1982) for details]; λ_v is weighted coefficients optimizing grids variation in cell volumes; W is a given function by which the density of computation grids can be adjusted. To generate a grid, finite difference approximations to the Euler equations are solved by iteration.

FINITE DIFFERENCE PROCEDURE

A staggered grid scheme in the ξ-η plane is employed as shown in Fig. 2. $\times$ denotes a ζ-

point at which ζ and P are computed, ○ denotes a u-point at which $\tilde{u}$, U and u are computed and □ denotes a v-point at which $\tilde{v}$, V and v are computed. The separate labeling for ζ, u and

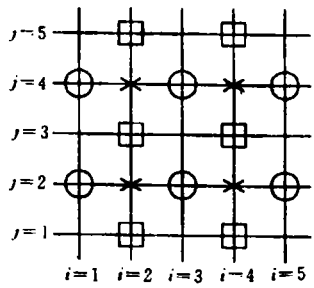

Fig. 2. Grid point arrangement.

v in this scheme is convenient for realizing boundary conditions. The new coordinates (ξ, η) are taken as integer grid positions, $\xi = 1, 2\cdots, m$, $\eta = 1, 2\cdots, n$, where m and n are chosen to be even so that there are only u-points at Π_1, Π_2, where $U = 0$ is satisfied, and only v-points at Π_3, Π_4, where $V = 0$.

The discretizations of Eqs (18)~(20) are in the forms of semi-implicit scheme as described in the SAM model (Shi and Sun, 1995). Equation (22) is solved by the splitting operator method. The first step is the advection procedure in which the upwind scheme is adopted, and the second is the diffusion procedure with the center-difference scheme. It has been proved that the discretizations of this kind of conservational equations have good accuracy and numerical stability (Shi and Sun, 1995)

Many nearshore areas contain tidal flats. These areas are dry during low water and flooded when the tide rises. In the numerical model the process of drying and flooding is represented by removing grid points from the flow domain when the tide falls and by adding grid points when the tide rises. This method is more similar to WDM method used in the computation of storm surge flooding (Shi *et al.*, 1996). In the present model, Eq. (18) is used in the updating procedure at all ζ- points even at dry points because at these dry points, $U = 0$ and $V = 0$ result in $\Delta_t\zeta = 0$, i. e., there is no variation of the water surface elevation in dry cells. Equations (19) and (20) are used for updating u and $\tilde{v}$ respectively at wet points, and then values of u and v are deduced from Eq. (21). The wet or dry grid points must be judged by the prescribed criterion as described in

the WDM model (Shi *et al.*, 1996).

AN APPLICATION IN THE YANGPU BAY AND THE XINYING BAY

The Yangpu Bay and the Xinying Bay, which are located between latitudes 19°30′ and 20°00′ N and longitudes 109°00′ and 109°20′ E, are connected by a narrow channel as shown in Fig. 3. The coastlines and the topographies are more complex, and the narrow channel is only 600 m wide. The Xinying Bay contains shallow areas with wide tidal flats, and two river mouths, i.e., the Beimen River mouth and the Chunjiang River mouth. Because a lot of waste water is discharged into the rivers and the rivers are lack of self-purification capability, the river mouths then become the inlets of the sources of industry pollutants. Among the pollutants released from

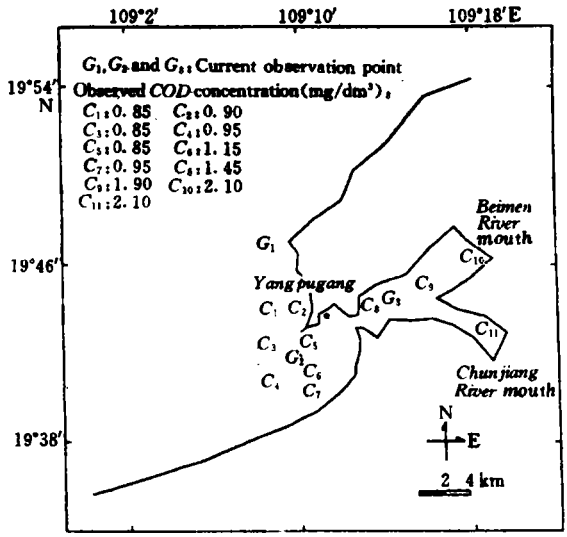

Fig. 3. Analysed area and position of observations.

the river mouths, *COD* concentration accounts for a large proportion. According to the investigations, the Beimen River mouth releases *COD* at a mean rate of 30.82 g/s and the Chunjiang River mouth at a rate of 90.03 g/s. Figure 3 shows the investigated *COD* concentration values at the observation stations (C_1 – C_{11}) in the two bays.

In this paper, the tidal currents of three main tidal constituents O_1, K_1 and M_2 are simulated by using the BFG model. And then the current results are used to calculate the distribution of *COD* concentration in the area. The results are finally compared with the observed data.

Figure 4 shows the grid mesh generated by means of the self-adaptive grid generation method. In the generating process, the parameter W must be adjusted several times in order to get a varying spacing grid with grid smoothness and orthogonality. The values of W in the narrow channel is larger than other areas so that the grid in the part is the finest. In the present grid mesh, the smallest grid spacing is 55 m at the narrow channel and the largest grid spacing is 1195 m at the open boundary.

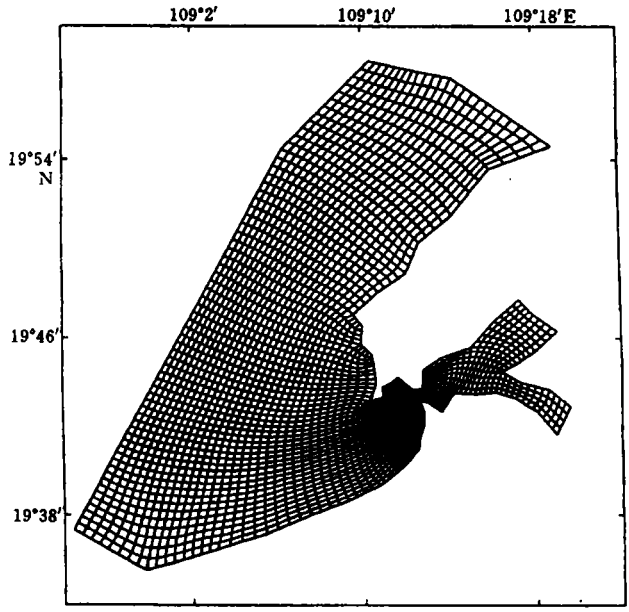

Fig. 4. Generated grid mesh.

In the calculation of tidal currents, the tidal levels on the open boundaries are provided by the results from the large region model with large grid spacings. In order to test the calculation accuracy, the comparison between the calculated results and the observed data should be made. Figures 5 a, b and c show calculated and observed tidal level curves of O_1, K_1 and M_2 respectively at the tidal observatory at Yangpugang. And the tidal current testament of the three main tidal constituents are also made, and the comparison between calculated and observed results of O_1 at the observation points (G_1, G_2, G_3) are shown in Fig. 6. Figures 7 a and b show the current distributions of O_1 at the middle time of flood and ebb respectively. The current distributions of K_1 are similar to that of O_1 and the current of M_2 is smaller than that of O_1 and K_1, which are not

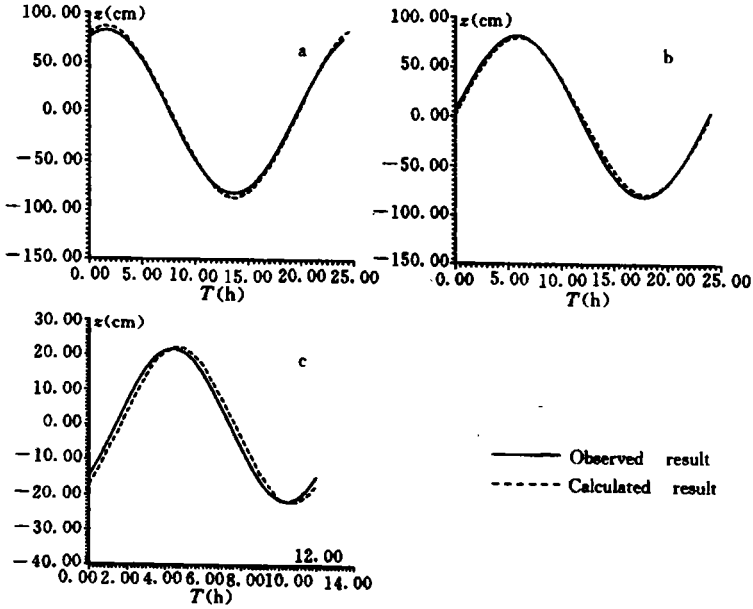

Fig. 5. Calculated and observed tidal levels at Yangpugang. a. O_1, b. K_2 and c. M_2.

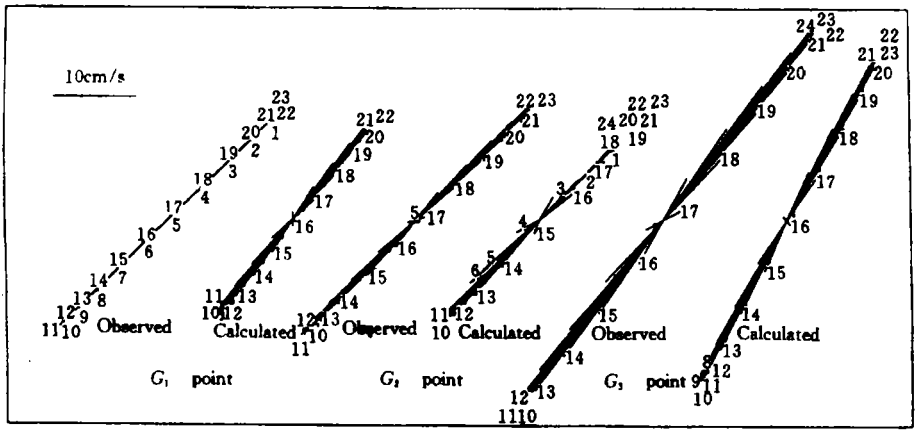

Fig. 6. Comparisons between calculated tidal currents and observations of O_1.

shown in the paper. Figure 7 also shows that the maximum current velocity appears in the narrow channel.

In the calculation of the *COD* concentration, m_1 tidal current together with the M_2 current are adopted as the advection velocity. Figure 8 shows the calculated distribution of the *COD* con-

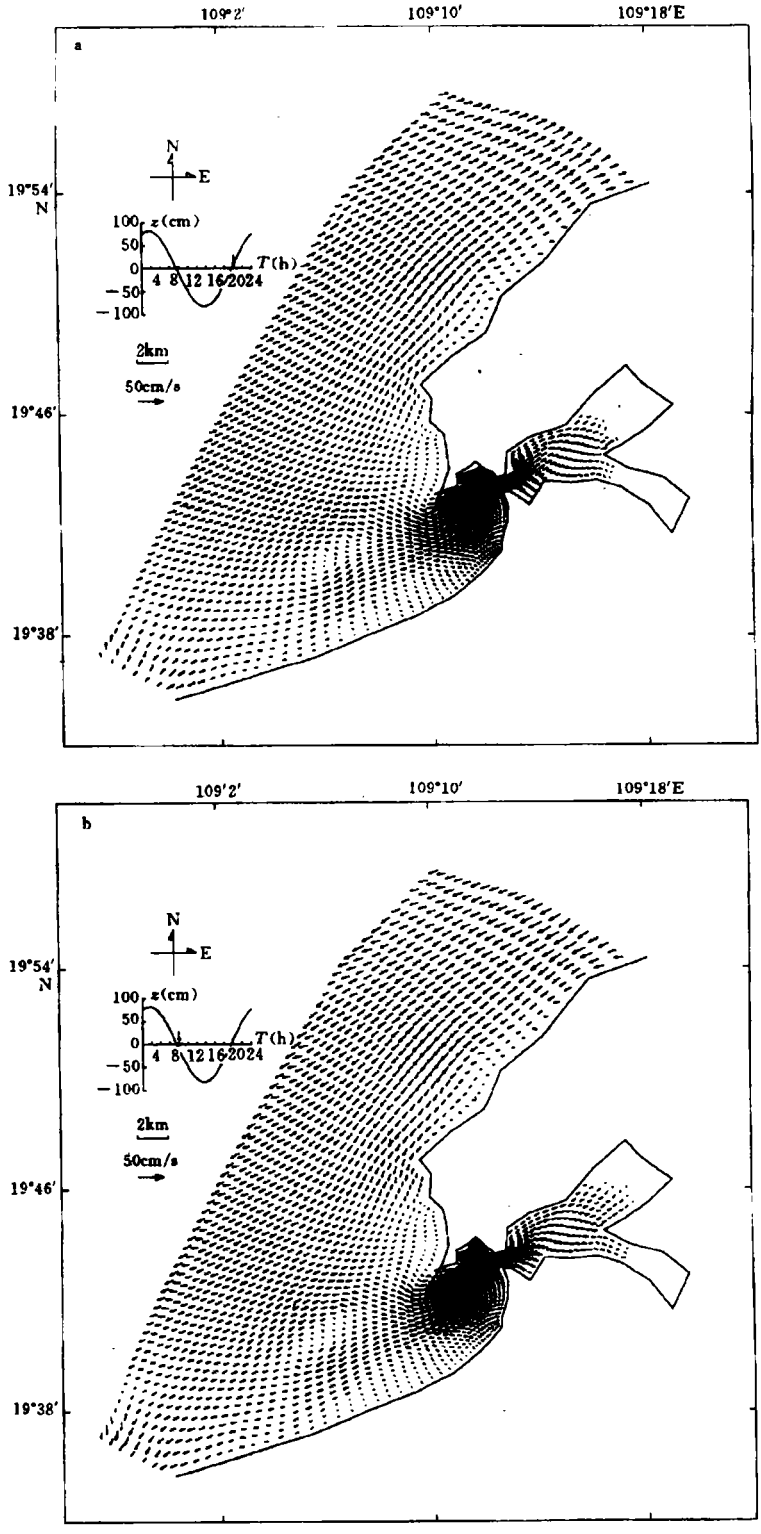

Fig. 7. Current distributions of O_1 at the middle time of flood tide (a) and at the middle time of ebb tide (b).

centration. As compared with the observed data as shown in Fig. 3, the result seems fairly good.

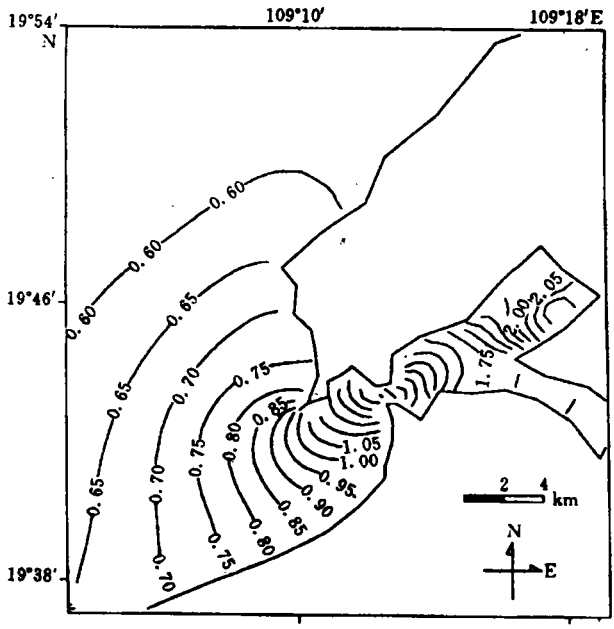

Fig. 8. Distribution of *COD* concentration.

CONCLUSION

Generalized dynamic governing equations of tidal motions and the advection diffusion equation of pollutants in curvilinear coordinates are derived in this study, and consequently the varying spacing and boundary-fitted grid mesh, which is fine in the coastal region especially in a narrow channel and coarse in the offshore region, can be conveniently adopted. In the equations, the contravariant components of the velocity vector, which are taken as the generalized velocities in the image plane, are introduced. Such introduction not only easily realizes the boundary condition in curvilinear coordinates, but also makes the transformed equations conservational, which is more useful for the finite difference computation. Finally the self-adaptive grid method is employed to generate varying spacing curvilinear grids in the Yangpu Bay and the Xinying Bay, and the verification calculations of the tidal currents and *COD* concentration in the area have proved this model to be an effective one for the calculation in more complex nearshore areas.

REFERENCES

Brackbill J. U. and J. S. Saltzman (1982) Adaptive zoning for singular problems in two dimensions. *Journal of Computational Physics*, **46**, 342～368.

Dortch M. S., S. C. Raymond and R. A. Steven (1992) Application of three-dimensional Lagrangian residual transport. *Journal of Hydraulic Engineering*, **118**(6), 831～848.

Lynch and Gray (1980) Finite element simulation of fluid in deforming region. *Journal of Computational Physics*, **39**, 135～153.

Medina D., A. B. Liggett and K. Torrence (1991) A consistent boundary element method for free surface hydrodynamic calculations. *International Journal for Numerical Methods in Fluids*, **12**, 835～857.

Shi Fengyan and Sun Wenxin (1995) A variable boundary model of storm surge flooding in generalized curvilinear grids. *International Journal for Numerical Methods in Fluids*, **21**, 641～651.

Shi Fengyan, Sun Wenxin and Wei Gengsheng (1996) (In press) A WDM method on generalized curvilinear grid for calculation of storm surge flooding. *Applied Ocean Research*.